

Article

Effects of Temperature-Dependent Conductivity and Magnetic Field on the Radiated Carreau Nanofluid Flow and Entropy Generation

Sami Ullah Khan ¹, Imen Safra ², Kaouther Ghachem ² , Hind Albalawi ³, Taher Labidi ⁴ and Lioua Kolsi ^{5,*} ¹ Department of Mathematics, Namal University, Mianwali 42250, Pakistan; sk_iuu@yahoo.com² Department of Industrial and Systems Engineering, College of Engineering, Princess Nourah bint Abdulrahman University, P.O. Box 84428, Riyadh 11671, Saudi Arabia; imsafra@pnu.edu.sa (I.S.); kgmaatki@pnu.edu.sa (K.G.)³ Department of Physics, College of Sciences, Princess Nourah bint Abdulrahman University, P.O. Box 84428, Riyadh 11671, Saudi Arabia; hmalbalawi@pnu.edu.sa⁴ Department of Software Engineering, College of Computer Engineering and Sciences, Prince Sattam bin Abdulaziz University, P.O. Box 151, Al-Kharj 11942, Saudi Arabia; t.labidi@psau.edu.sa⁵ Department of Mechanical Engineering, College of Engineering, University of Ha'il, Ha'il 81451, Saudi Arabia
* Correspondence: lioua_enim@yahoo.fr

Abstract: This investigation is related to this study of entropy generation during Carreau nanofluid flow under variable thermal conductivity conditions. The heat and mass transfer phenomena are observed in the presence of thermal radiation and activation energy. The flow is induced by a porous stretching surface. Appropriate variables are used in order to simplify the problem into dimensionless form. The numerical simulations are performed by using the shooting technique. The physical aspects of the problem in view of different flow parameters are reported. It is observed that consideration of variable fluid thermal conductivity enhances heat transfer. An enhancement in heat and mass transfer phenomena is observed with increasing the Weissenberg number. Moreover, entropy generation increases with Weissenberg and Brinkman numbers. Current results present applications in thermal processes, heat exchangers, energy systems, combustion and engine design, chemical processes, refrigeration systems, etc.

Keywords: Carreau nanofluid; entropy generation; activation energy; variable thermal conductivity; porous surface



Citation: Khan, S.U.; Safra, I.; Ghachem, K.; Albalawi, H.; Labidi, T.; Kolsi, L. Effects of Temperature-Dependent Conductivity and Magnetic Field on the Radiated Carreau Nanofluid Flow and Entropy Generation. *Symmetry* **2023**, *15*, 1847. <https://doi.org/10.3390/sym15101847>

Academic Editor: Taher Armaghani

Received: 30 August 2023

Revised: 22 September 2023

Accepted: 26 September 2023

Published: 30 September 2023



Copyright: © 2023 by the authors. Licensee MDPI, Basel, Switzerland. This article is an open access article distributed under the terms and conditions of the Creative Commons Attribution (CC BY) license (<https://creativecommons.org/licenses/by/4.0/>).

1. Introduction

During the last few decades, many technological and industrial applications were improved and restructured with the aid of nanotechnology, which is widely used in medicine, information technology, nuclear science, environmental science, and many others. Because of the unique properties of nanofluids, which make them certainly useful in many implementations and utilizations of heat transfer processes, including biomedicine, microchannel flow, heating and cooling processes, chillers, boilers, and many others, the thermal conductivity and heat transfer rate are highly enhanced by using nanofluids in comparison with base fluids. Presently, scientists and engineers are augmenting the future entanglement of nanotechnology. Many new materials and devices could be created and invented with the help of nanotechnology, which has a wide scope of usefulness and utilization, e.g., in nanoweapons, nanometrology, biomaterials, etc. Irfan et al. [1] analyzed Carreau nanofluid theoretically with MHD and Arrhenius activation energy. The consequences of mass flux theory are also discussed. Hisao [2] focused on Carreau nanofluid with thermal radiation, MHD, and activation energy. Khan et al. [3] examined the flow of the Carreau nanofluid and estimated the irreversibility analysis. Waqas et al. [4] deduced the thermal reflection associated with Carreau nanofluid from the contribution

of radiative phenomena. Ullah et al. [5] depicted the rotating behavior of nanofluid flow containing ternary tiny particles regarding the thin film phenomenon. Muhammad et al. [6] observed the carbon nanotubes flow with squeezing flow constraints subjecting to boost the water base properties. Rasool and Wakif [7] identified the EMHD flow regarding the second-grade nanofluid over Riga space. Alqarni et al. [8] observed the bioconvection concept for nanofluids with melting heating transfer features. Borbora et al. [9] presented detailed review contributions for nanofluid associated with the cavity geometry. Acharya [10] discussed the copper-water-decomposed nanomaterial thermal activities with optimized impact. Shamshuddin et al. [11] utilized the observations to assess the heat transfer determination due to ferro-oxide nanoparticles. Negi et al. [12] deduced the observations for nanofluids subjected to zero-mass conditions. The hybrid nanofluid flowing in a channel with suction phenomenon was conducted by Maiti et al. [13]. Mabood et al. [14] used Wu's slip impact for Williamson nanofluid flow with microorganisms.

The phenomenon of entropy generation is associated with the control of energy loss in various thermal phenomena and cooling systems. The appearance of entropy generation is commonly observed in thermodynamic processes where there is a transfer of heat and energy in an irreversible process due to temperature differences. According to the second theory of thermodynamics, an enhancement in the entropy of isolated systems is boosted over time or remains constant in ideal reversible systems. The concept of entropy generation is an exhibition of this theory and refers to the irreversibility of various processes. In real-world applications, the entropy generation phenomenon is linked to the loss of thermal processes in heat transfer systems. In the case of heat engines, the conversion of energy from one system to another yields a loss of water and increases entropy. This waste heat represents an increase in the disorder of the system and its surroundings. Understanding and managing entropy generation is crucial in engineering, as it allows for the optimization of processes to minimize losses and increase overall system efficiency. By identifying the sources of entropy generation, engineers can design more efficient systems, develop better insulation, improve heat exchangers, and implement strategies to reduce energy waste. Makhdoum et al. [15] investigated the Lorentz force and entropy generation assessed for an inclined surface with nanoparticles. Li et al. [16] explored the slip onset for optimized nanofluid Jeffrey nanofluid flow numerically. Shah et al. [17] reported the optimized production of $\text{NiZnFe}_2\text{O}_4$ and $\text{MnZnFe}_2\text{O}_4$ nanoparticles on curved surfaces. Micropolar nanofluid following pulsating motion in view of entropy generation applications was predicted by Rajkumar et al. [18]. Derikv et al. [19] reported the entropy production assessment for MWCNTs- Fe_3O_4 decompositions.

Based on the above-described references, it can be concluded that several scientists have studied the effect of the thermal properties of nanofluids on flow and temperature fields. In most of the available investigations, the thermal conductivity of nanomaterials is assumed to be constant. However, it is observed that in many thermal processes, the thermal conductivity of nanomaterials fluctuates. Therefore, the aim of current research is to examine heat and mass transfer, fluid flow, and entropy generation during Carreau nanofluid flow with variable thermal conductivity. The assessment of heat and mass transfer phenomena is considered in the presence of thermal radiation and activation energy effects. The porous moving surface with magnetic force interaction induces a uniform, steady flow. The motivations for considering the Carreau fluid model are due to its interesting rheology and viscoelastic properties and to its diverse applications in engineering and industrial sectors. It allows engineers and scientists to predict and analyze the flow characteristics of non-Newtonian fluids, which is essential for the design and optimization of processes involving such fluids, including polymer processing, food processing, and various other industrial applications.

2. Model Development

The bidirectional flow of the Carreau nanofluid is assumed to be due to the porous, stretched surface. The stretching phenomenon is occurring along the x and y , directions

and an external magnetic field is applied along the z direction. The velocity components u are assigned along the x direction, v is assumed along the y axis, and w is taken in the z direction, as shown in Figure 1. Fluid thermal conductivity is considered temperature-dependent. In addition, the effects of radiative heat transfer and activation energy are considered in the energy and concentration equations, respectively. The stress tensor for incompressible Carreau nanofluid is given by [20,21]:

$$\sigma_{ij} = \left[\epsilon_{\infty} + (\epsilon_0 - \epsilon_{\infty}) \left(1 + (\Pi \beta^{\circ})^2 \right)^{\frac{n-1}{2}} \right] A_1 \tag{1}$$

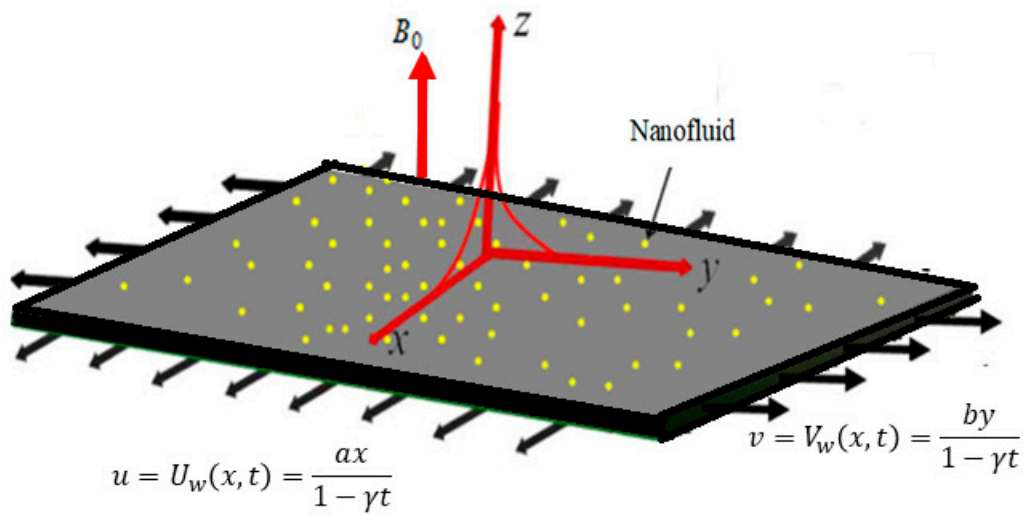


Figure 1. Geometry of the problem.

Here ϵ_{∞} and ϵ_0 denote the viscosities at infinite shear rate and zero shear rate, respectively. Π denotes the rate for material flexibility. A_1 is the first Rivlin-Ericksen tensor. n represents the behavior index.

$$\beta^{\circ} = \sqrt{\frac{1}{2}(\text{trace } A_1)^2}. \tag{2}$$

The governing equations are modeled as [20,21]:

$$\frac{\partial u}{\partial x} + \frac{\partial v}{\partial y} + \frac{\partial w}{\partial z} = 0, \tag{3}$$

$$\begin{aligned} & \frac{\partial u}{\partial t} + u \frac{\partial u}{\partial x} + v \frac{\partial u}{\partial y} + w \frac{\partial u}{\partial z} \\ &= v \frac{\partial^2 u}{\partial z^2} \left[1 + \Pi^2 \left(\frac{\partial u}{\partial z} \right)^2 \right]^{\frac{n-1}{2}} + v(n-1) \Pi^2 \left(\frac{\partial u}{\partial z} \right)^2 \frac{\partial^2 u}{\partial z^2} \left[1 + \Pi^2 \left(\frac{\partial u}{\partial z} \right)^2 \right]^{\frac{n-3}{2}} \\ & - \left(\frac{\tilde{\sigma} B_0^2}{\rho} u + \frac{v}{K_1} u \right), \end{aligned} \tag{4}$$

$$\begin{aligned} & \frac{\partial v}{\partial t} + u \frac{\partial v}{\partial x} + v \frac{\partial v}{\partial y} + w \frac{\partial v}{\partial z} \\ &= v \frac{\partial^2 v}{\partial z^2} \left[1 + \Pi^2 \left(\frac{\partial v}{\partial z} \right)^2 \right]^{\frac{n-1}{2}} + v(n-1) \Pi^2 \left(\frac{\partial v}{\partial z} \right)^2 \frac{\partial^2 v}{\partial z^2} \left[1 + \Pi^2 \left(\frac{\partial v}{\partial z} \right)^2 \right]^{\frac{n-3}{2}} \\ & - \left(\frac{\tilde{\sigma} B_0^2}{\rho} v + \frac{v}{K_1} v \right) \end{aligned} \tag{5}$$

$$\begin{aligned} & \frac{\partial T}{\partial t} + u \frac{\partial T}{\partial x} + v \frac{\partial T}{\partial y} + w \frac{\partial T}{\partial z} \\ &= \frac{1}{(\rho c)_f} \frac{\partial}{\partial z} \left(K_{nf}(T) \frac{\partial T}{\partial z} \right) + \tau \left[D_B \left(\frac{\partial C}{\partial z} \frac{\partial T}{\partial z} \right) + \frac{D_T}{T_{\infty}} \left(\frac{\partial T}{\partial z} \right)^2 \right] - \frac{1}{(\rho c)_f} \frac{\partial q_r}{\partial z}, \end{aligned} \tag{6}$$

$$\frac{\partial C}{\partial t} + u \frac{\partial C}{\partial x} + v \frac{\partial C}{\partial y} + w \frac{\partial C}{\partial z} = D_B \frac{\partial^2 C}{\partial z^2} + \frac{D_T}{T_\infty} \frac{\partial^2 T}{\partial z^2} - K_r^2 \left(\frac{\tilde{T}}{\tilde{T}_\infty} \right)^n \exp \left(\frac{-Ea}{K_{nf} \tilde{T}} \right) (\tilde{C} - \tilde{C}_\infty), \tag{7}$$

The temperature dependent thermal conductivity $K_{nf}(T)$, is expressed via the following relation [14]:

$$K_{nf}(T) = K_{nf} \left(1 + \epsilon_1 \frac{T - T_\infty}{T_w - T_\infty} \right) \tag{8}$$

with a small parameter (ϵ_1). The radiative flux q_r is defined as [14]:

$$q_r = - \frac{4\sigma^*}{3k^*} \frac{\partial T^4}{\partial z}, \tag{9}$$

with σ^* is the Stephen Boltzmann constant.

The boundary conditions are:

$$u = U_w(x, t) = \frac{ax}{1 - \gamma t}, v = V_w(x, t) = \frac{by}{1 - \gamma t}, w = 0, T = T_w, C = C_w \text{ at } z = 0, \tag{10}$$

$$u \rightarrow 0, v \rightarrow 0, T \rightarrow T_\infty, C \rightarrow C_\infty \text{ as } z \rightarrow \infty. \tag{11}$$

Introducing new transformations [20,21]:

$$u = \frac{ax}{1 - \gamma t} f'(\eta), v = \frac{ay}{1 - \gamma t} g'(\eta), w = - \sqrt{\frac{va}{1 - \gamma t}} (f(\eta) + g(\eta)), \eta = \sqrt{\frac{a}{v(1 - \gamma t)}} z, \tag{12}$$

$$\theta(\eta) = \frac{T - T_\infty}{T_w - T_\infty}, \varphi(\eta) = \frac{C - C_\infty}{C_w - C_\infty}$$

New system is:

$$f''' \left[1 + We_1^2 f''^2 \right]^{\frac{n-3}{2}} \left[1 + nWe_1^2 f''^2 \right] + (f + g) f'' - f'^2 - S(f' + \eta/2 f'') - (M^2 + K) f' = 0, \tag{13}$$

$$g''' \left[1 + We_2^2 g''^2 \right]^{\frac{n-3}{2}} \left[1 + nWe_2^2 g''^2 \right] + (f + g) g'' - g'^2 - S(g' + \eta/2 g'') - (M^2 + K) g' = 0, \tag{14}$$

$$(1 + (4/3) Rd + \theta) \theta'' + \epsilon \theta'^2 + Pr \left[(f + g) \theta' - S \{ \theta' + \eta/2 \theta'' \} + Nt \theta'^2 + Nb \theta' \varphi' \right] = 0, \tag{15}$$

$$\varphi'' + (N_t/N_b) \theta'' + PrLe \left[(f + g) \varphi' - (1/2) \eta S \varphi' \right] - \sigma Sc (1 + \gamma \theta)^n \exp \left(- \frac{E}{1 + \gamma \theta} \right) \varphi = 0, \tag{16}$$

with:

$$f(0) = 0 = g(0), \varphi(0) = 1, \theta(0) = 1, f'(0) = 1, g'(0) = \alpha_1, \tag{17}$$

$$f'(\infty) \rightarrow 0, g'(\infty) \rightarrow 0, \varphi(\infty) \rightarrow 0, \theta(\infty) \rightarrow 0. \tag{18}$$

where $We_1 = \sqrt{\frac{a(\Gamma U_w)^2}{v}}$ and $We_2 = \sqrt{\frac{a(\Gamma V_w)^2}{v}}$ are Weissenberg numbers, $S = \frac{\gamma}{a}$ is unsteadiness parameter. $K = \frac{v}{aK_1}$ is the porosity parameter, $M = \frac{\sigma B_0^2}{a\rho}$ represents magnetic number, $Rd = \frac{4\sigma^* \tilde{T}_\infty^3}{k^* K_{nf}}$ specifies the radiation parameter, $Pr = \frac{v}{\alpha_m}$ denotes Prandtl number, $Nt = \frac{\tau D_T (T_w - T_\infty)}{v}$ represents thermophoresis, $Nb = \frac{\tau D_b (C_w - C_\infty)}{v}$ indicates Brownian movement and $E = \frac{Ea}{K_{nf} T_\infty}$ is the activation energy, $\gamma = \frac{(T_w - T_\infty)}{T_w}$ is the temperature difference

parameter and $\sigma = \frac{K_{nf}^2 x}{\nu}$ is the chemical reaction parameter whereas the ratio of stretching rates is represented by $\alpha_1 = \frac{b}{a}$. Defining important engineering quantities:

$$C_{fx} = \frac{\tau_{xz}}{\frac{1}{2}\rho(U_w)^2}, C_{fy} = \frac{\tau_{yz}}{\frac{1}{2}\rho(V_w)^2}, Nu_x = -\frac{x}{K(T_w - T_\infty)} \left(\frac{\partial T}{\partial z} \right)_{z=0} + \frac{xq_r}{\lambda(T_w - T_\infty)},$$

$$Sh_x = -\frac{x}{D_C(C_w - C_\infty)} \left(\frac{\partial C}{\partial z} \right)_{z=0}. \tag{19}$$

Here τ_{xz} and τ_{yz} specify stress along x and directions, y respectively, q_r represents the radiative flux on a stretched surface. The above-stated quantities are reformed through similarity transformation into dimensionless form as follows:

$$\frac{1}{2} \sqrt{Re_x C_{fx}} = f''(0) \left[1 + We_1^2 f''^2(0) \right]^{\frac{n-1}{2}}, \tag{20}$$

$$\frac{1}{2} \frac{U_w}{V_w} \sqrt{Re_y C_{fy}} = g''(0) \left[1 + We_2^2 g''^2(0) \right]^{\frac{n-1}{2}}, \tag{21}$$

$$\frac{Nu_x}{\sqrt{Re_x}} = -\left(1 + \frac{4}{3} Rd \right) \theta'(0), \tag{22}$$

$$\frac{Sh_x}{\sqrt{Re_x}} = -\phi'(0). \tag{23}$$

where $(Re_x = \frac{xU_w}{\nu})$.

3. Entropy Generation

The S_g''' is denoting the entropy generation, combining the viscous dissipation, heat, and mass transfer, and the Joule effect irreversibility is given by [3]:

$$S_g''' = \frac{K_{nf}}{T_w^2} \left[\left(\frac{\partial T}{\partial z} \right)^2 + \frac{16\sigma^* T_\infty^3}{3k^* K_{nf}} \left(\frac{\partial T}{\partial z} \right)^2 \right] + \frac{\mu}{T_w} \left[2 \left(\frac{\partial u}{\partial x} \right)^2 + 2 \left(\frac{\partial u}{\partial y} \right)^2 + \left(\frac{\partial u}{\partial x} + \frac{\partial u}{\partial y} \right)^2 \right] + \frac{\tilde{\sigma} B_0^2}{T_w} (u^2 + v^2) + \frac{R_g K_c}{C_w} \left(\frac{\partial C}{\partial z} \right)^2, \tag{24}$$

The first term corresponds to thermal irreversibility caused by the temperature gradient. The second term corresponds to frictional entropy generation. The third term denotes irreversibility caused by magnetic effects (the Joule effect). The fourth term is irreversibility caused by mass diffusion. The characteristic entropy generation is given by [3]:

$$S_0''' = \frac{K_{nf}(T_w - T_\infty)^2}{L^2 T_w^2}, \tag{25}$$

The entropy number (N_G) is nondimensionalized form obtained by taking the ratio of the rate of actual (S_g''') to characteristic entropy generation (S_0''').

$$N_G = \frac{\check{K}}{\Lambda_1} \left(\Lambda_1 \left(1 + \frac{4}{3} Rd \right) \theta'^2 + \Gamma_1 \left(\theta' + \frac{\Lambda_2}{\Lambda_1} \phi' \right) \phi' + \Gamma_2 (Br_1 f'^2 + Br_2 g'^2) \right) + 2 (Br_1 f''^2 + Br_2 g''^2) \tag{26}$$

4. Numerical Computations

The dimensionless form of the governing equations is presented in Equations (13)–(16), satisfying the boundary conditions (17–18). Due to its extremely complicated nature, this system cannot be treated via an exact solution approach. To solve this problem, the fourth-order Runge-Kutta method (RK-4) is used to obtain an approximate solution. This numerical scheme is quite accurate and can be implemented easily to solve complicated

problems [18–21]. The rK4 scheme is an explicit numerical tool that can compute the solution to a problem at distinct time steps. In order to implement this scheme on a defined problem, the boundary conditions are converted into an initial value system as follows:

$$(X, Y_1, Y_2, Y_3, Y_4, Y_5, Y_6, Y_7, Y_8, Y_9, Y_{10}) = (\eta, f, f', f'', g, g', g'', \theta, \theta', \varphi, \varphi') \tag{27}$$

$$Y_3' = \frac{1}{[1 + We_1^2 Y_3^2]^{\frac{n-3}{2}} [1 + nWe_1^2 Y_3^2]} \left[Y_2^2 - (Y_1 + Y_4)Y_3 + S(Y_2 + Y_3 X/2) + (M^2 + K)Y_2 + FY_2^2 \right], \tag{28}$$

$$Y_4' = Y_5, Y_5' = Y_6, \tag{29}$$

$$Y_6' = \frac{1}{[1 + We_2^2 Y_6^2]^{\frac{n-3}{2}} [1 + nWe_2^2 Y_6^2]} \left[Y_5^2 - (Y_1 + Y_4)Y_6 + S\left(Y_5 + \frac{X}{2}Y_6\right) + (M^2 + K)Y_5 + FY_5^2 \right], \tag{30}$$

$$Y_7' = Y_8, \tag{31}$$

$$Y_8' = \frac{1}{\left[1 + \frac{4}{3}Rd\right]} Pr \left\{ (Y_1 + Y_4 + S^*)Y_8 - Nt Y_8^2 - NbY_8Y_{10} \right\}, \tag{32}$$

$$Y_9' = Y_{10}, \tag{33}$$

$$Y_{10}' = -\frac{Nt}{Nb}Y_8' - PrLe(Y_1 + Y_4 - SX/2)Y_{10}, \tag{34}$$

$$Y_{11}' = Y_{12}, \tag{35}$$

Associated boundary conditions are:

$$Y_1(0) = 0, Y_2(0) = 1, Y_4(0) = 0, Y_5(0) = \alpha_1, Y_7(0) = 1, Y_9(0) = 1, \tag{36}$$

$$Y_2(\infty) = 0, Y_5(\infty) = 0, Y_9(\infty) = 0 \tag{37}$$

In order to solve the above-presented system (initial value problem), we shot for appropriate guesses to $Y_3(0), Y_6(0), Y_8(0), Y_{10}(0)$ and $Y_{12}(0)$. The MATLAB software is used to perform the simulations. The simulations are performed with an accuracy of 10^{-6} .

5. Verification of the Numerical Model

Table 1 presents the verification of the proposed numerical model by comparing the obtained results for $f''(0)$ with those of Sharidan et al. [22] and Chamkha et al. [23]. The comparison shows the agreement between the results and ensures the validity of the numerical model.

Table 1. Comparison of $f''(0)$ with the results of Sharidan et al. [22] and Chamkha et al. [23] for $We_1 = We_2 = \alpha = 0$.

S	Sharidan et al. [22]	Chamkha et al. [23]	Present Results
0.8	-1.261042	-1.261512	-1.26105
1.2	-1.377722	-1.378052	-1.37773
2.0	-1.587362	-	-1.58735

6. Results and Discussion

The physical insight into the problem is discussed in this section. The observations are predicted for Weissenberg number (We_1), unsteadiness parameter (S), magnetic parameter (M), porosity constraint (K), Prandtl number (Pr), variable thermal conductivity parameter

(ϵ) radiation constant (Rd), Brownian motion constraint (Nb), thermophoretic constraint (Nt), Lewis number (Le). Figure 2a reflects the change in velocity along x directions (f') and velocity along y - direction (g') due to variation of unsteady parameter S . Upon enhancing the impact of S , a decrement behavior is observed in both velocities. Such effects are associated with the nonlinear motion of a moving surface, which endorses the flow. The simulations performed for predicting the dynamic of f' and g' subject to Weissenberg number (We_1) have been reported in Figure 2b. The decrement resulted in f' and g' due to the uprising We_1 . Physically, the Weissenberg number reflects the role of inertial and viscous forces. Upon increasing the Weissenberg number, inertial forces become more dominant, which controls the velocity increment. The role of the Weissenberg number is important in assessing the rheology of a nonlinear fluid model. Further, in contrast to Figure 2a, the fluctuation in g' is more dominant. Figure 2c discloses the characteristics of the porosity parameter K on the distribution of f' and g' . The decreasing features of K are examined against f' and g' . Physically, such observational assessments are due to the permeability of tiny pores and the permeability of porous space. Figure 2d reports that f' and g' also decrease upon raising behavior index n . Moreover, the declining change in g' for increasing n are not prominent.

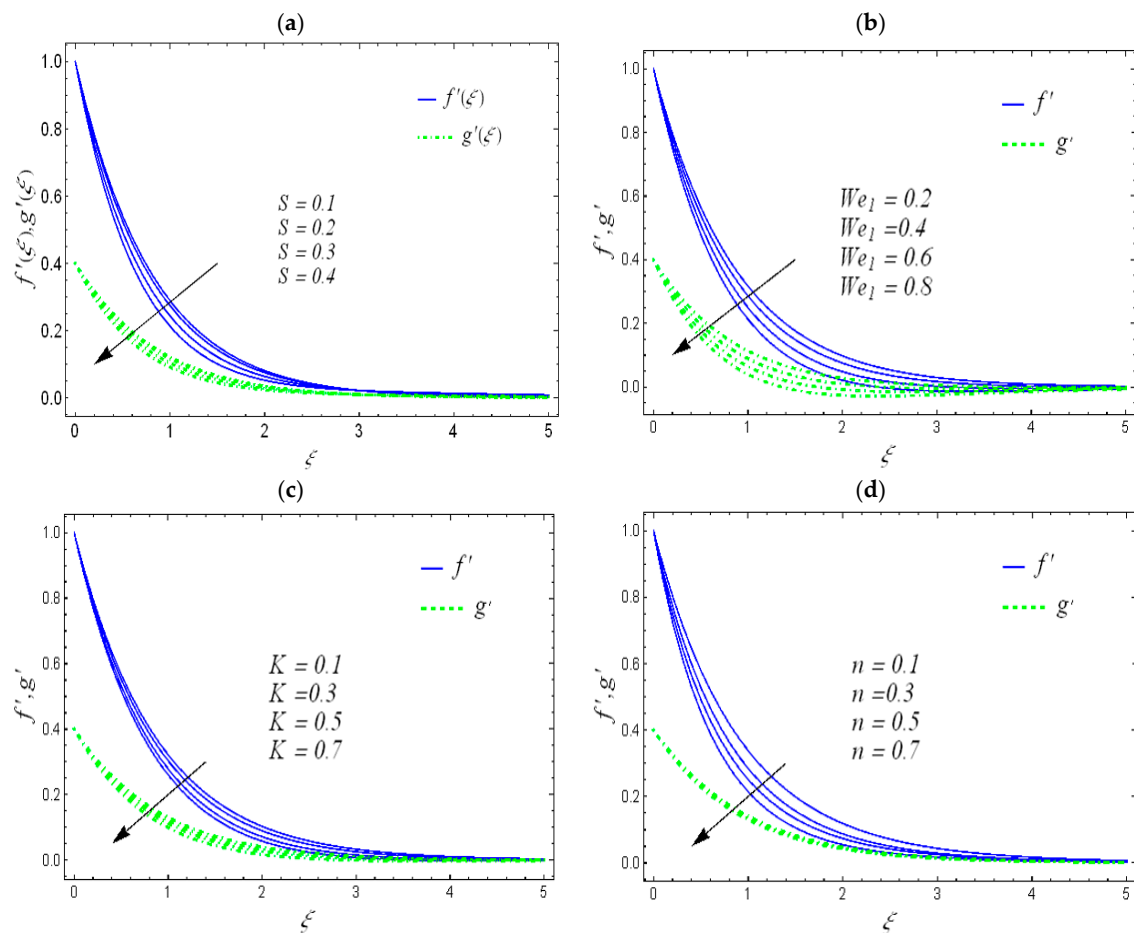


Figure 2. (a–d): Effects of S (a), We_1 (b), K (c) and n (d) on the vertical $f'(\eta)$ and horizontal $g'(\eta)$ velocity profiles.

Figure 3a suggests the significance of temperature profile θ for Weissenberg number We_1 . The maximum change in θ is associated with the peak values of We_1 . Physically, such outcomes are due to rheological forces. Figure 3b identifies the aspects of the unsteady parameter S on θ . The lower outcomes in the profile of θ due to S have been identified. The current fluid model is based on consideration of variable fluid viscosity, for which the role

of the variable thermal conductivity parameter is ϵ visualized in Figure 3c. The increasing applications of ϵ on θ are utilized. Therefore, it is clearly stated that thermal phenomena can be boosted when the fluid viscosity of materials is assumed to be temperature-dependent. Figure 3d encounters the consequences of the radiation parameter Rd on θ . The increasing assessment of the temperature profile is exhibited for the radiation constant. The radiative phenomenon is important in various thermal processes and engineering systems. The results explore the change in θ due to the Brownian motion constant Nb (Figure 3e). The Brownian parameter is a key factor in the nanofluid model, which discloses the random movement of nanoparticles. Due to such random motion, an increasing thermal profile is exhibited.

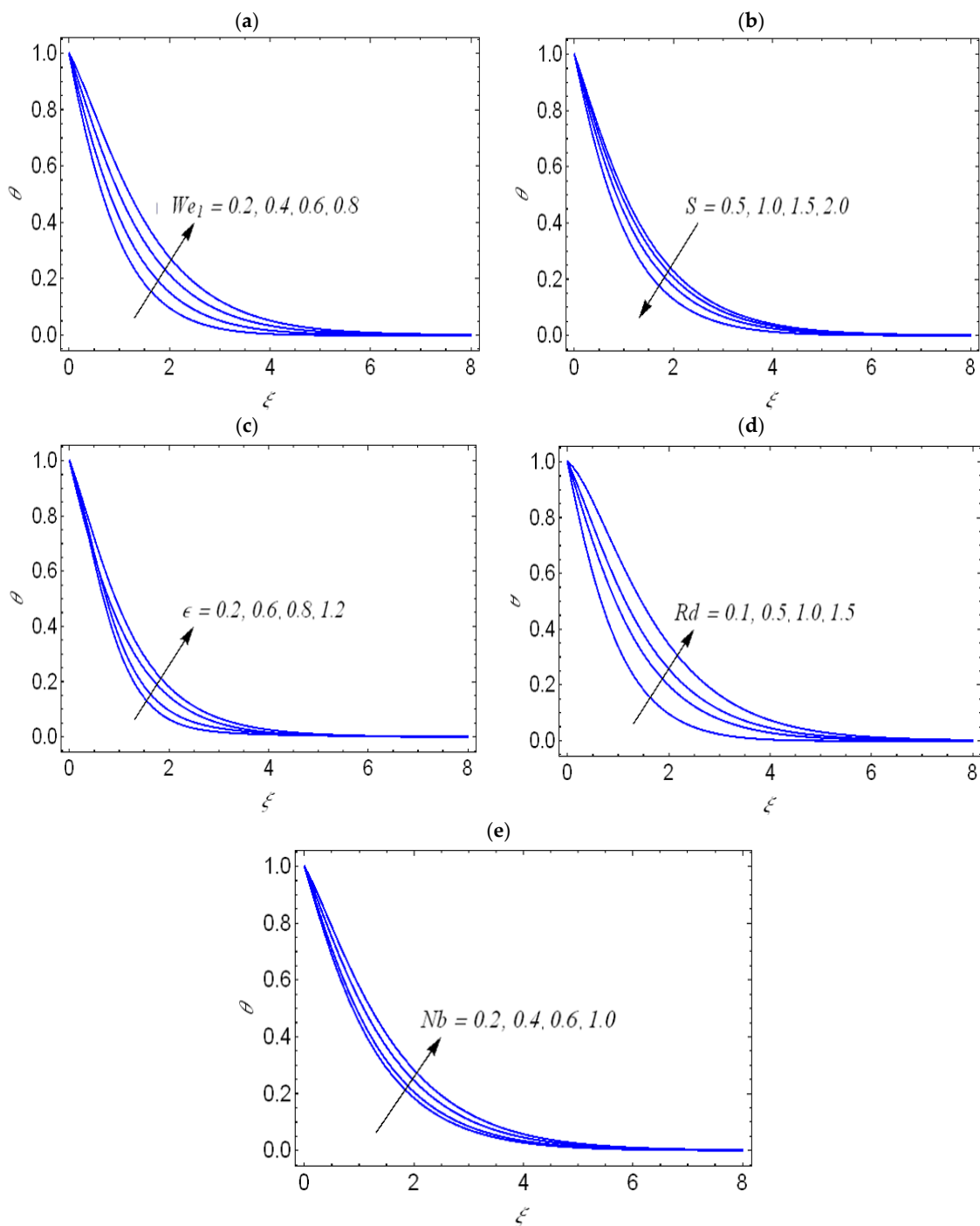


Figure 3. (a–e): Effects of We_1 (a), S (b), ϵ (c), Rd (d) and Nb (e) on the temperature profile θ .

Figure 4a concentrates on the change in concentration profile ϕ due to the deviation of the activation energy parameter E . An increase in ϕ is predicted with increasing the impact of E . Basically, the activation energy plays a vital role in initiating the chemical process. Figure 4b distributes the aspects of the thermophoresis parameter Nt on ϕ . An increasing outcome in ϕ against leading variation of Nt is encountered. The role of Schmidt number Sc on ϕ is illustrated in Figure 4c. The Schmidt number is subject to a reverse relation to mass diffusivity. The declining impact of ϕ with enhancing Sc slows down the mass diffusivity. The low fluctuation in mass diffusivity reduces the chemical process.

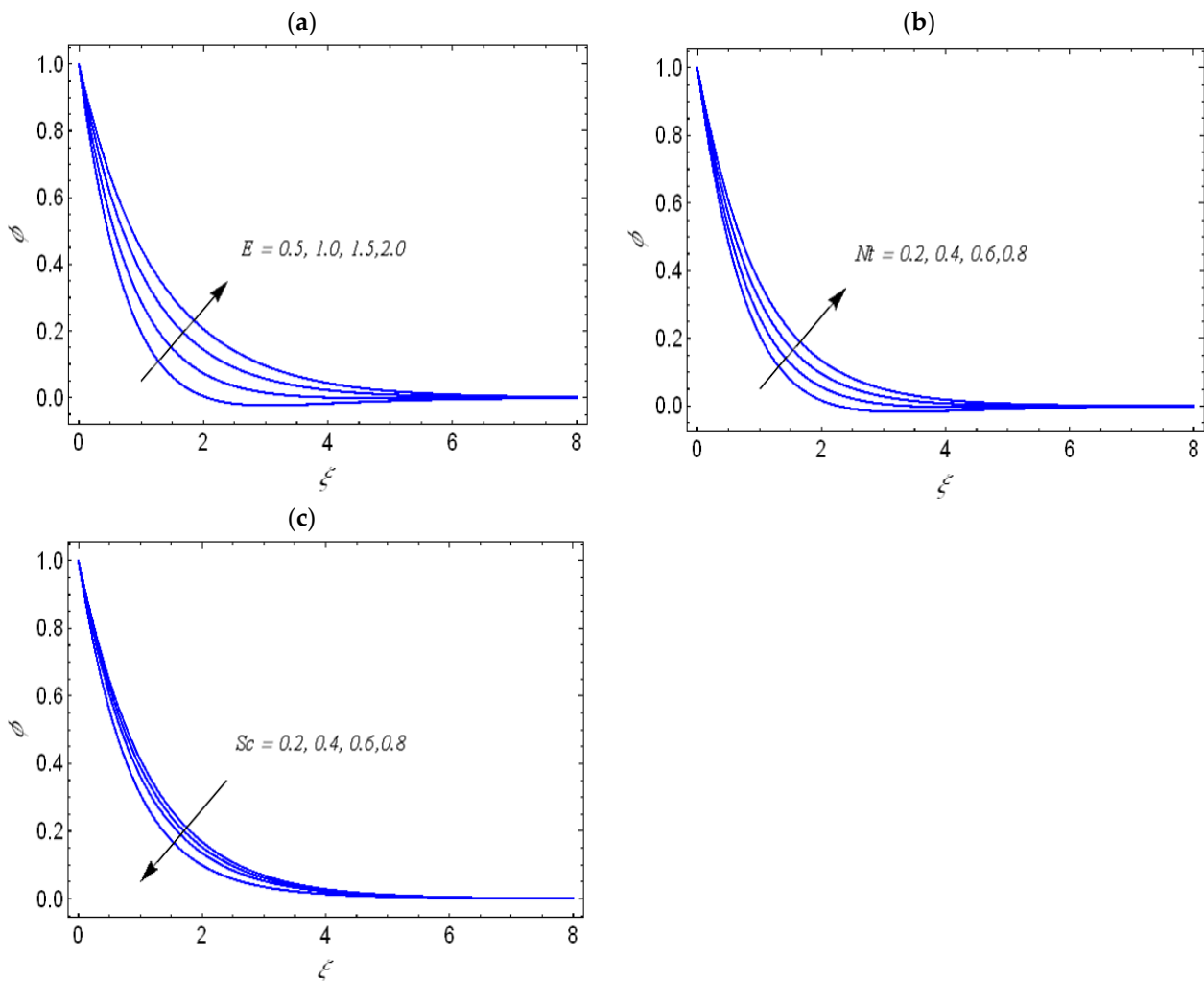


Figure 4. (a–c): Effects of E (a), Nt (b), and Sc (c), on the concentration profile ϕ .

Figure 5a identifies the change in entropy generation N_G for a larger Hartmann number M . The phenomenon of entropy generation is boosted when there is a meaningful change in M . Such features are due to the presence of Lorentz forces. Figure 5b utilized the contribution of Weissenberg number We_1 on N_G . It is noticed that the maximum entropy generation is referred to as larger We_1 . Since Weissenberg number displays the rheological impact of non-Newtonian fluid models, it is concluded that optimized phenomena can be controlled for non-Newtonian fluid models compared to viscous liquids. Figure 5c reported the change in N_G due to Brinkman number Br . The leading entropy generation is noted due to enhancing Br . Physically, the Brinkman number presents the ratio between fluctuations in heat transfer due to viscous dissipation and molecular conduction, and it plays a key role in polymer processing [24].

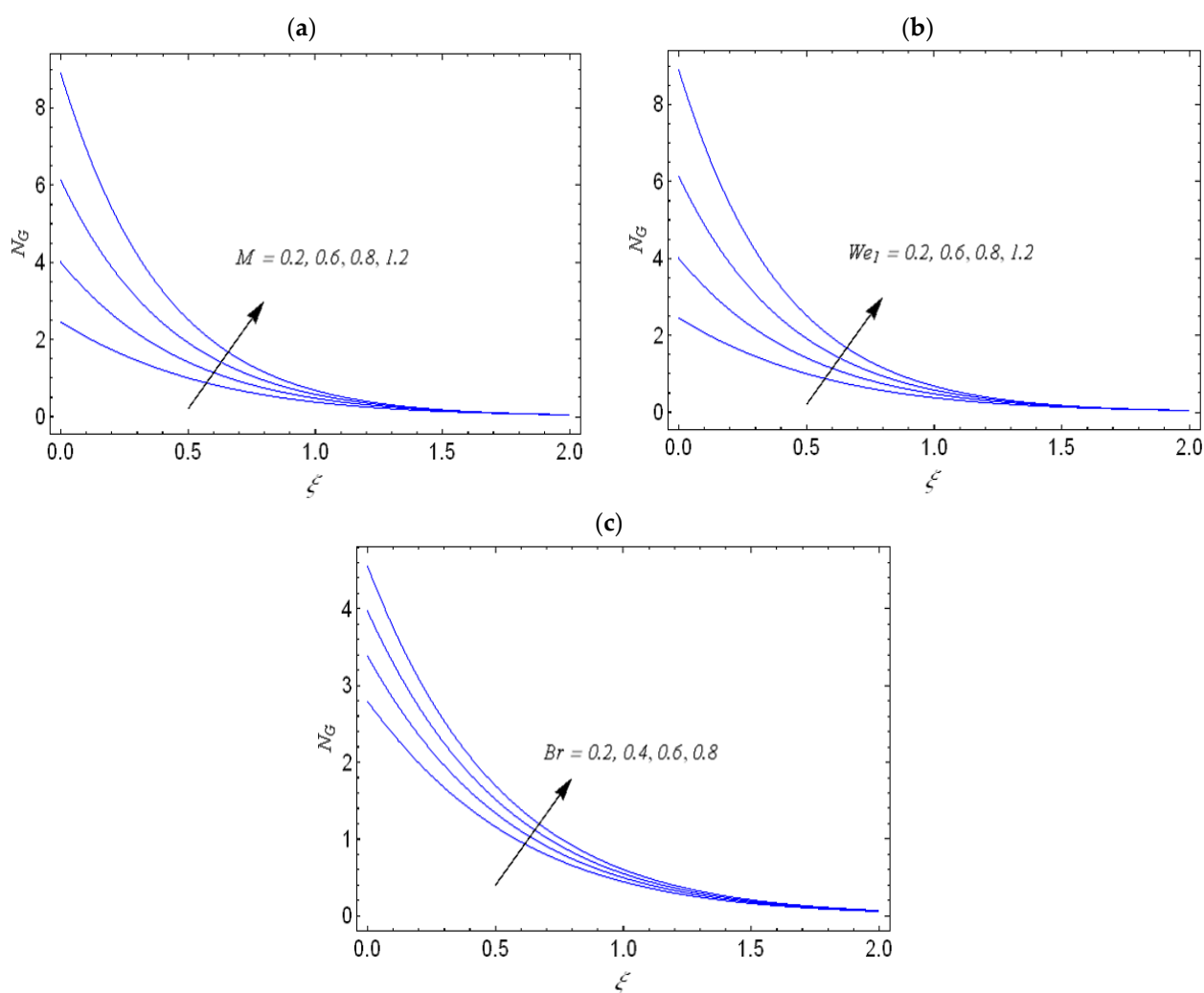


Figure 5. Effects of M (a), We_1 (b), and Br (c), on the local entropy generation N_G .

The numerical change in skin friction for a bidirectional stretching surface in view of the variation of flow parameters is observed in Table 2. Shear stress increases due to the MHD effect. Physically, such effects are related to the Lorentz force generated. Furthermore, an enhancement in skin friction coefficient is observed with material parameters. Such consequences are associated with the complex rheology of Carreau nanofluid.

Table 3 describes the change in Nusselt number and Sherwood number with Prandtl number Pr , unsteadiness parameter S , radiation constant, Hartmann number M , thermophoresis constant Nt and Brownian parameter Nb . The lowest value for both quantities occurs at higher values of the thermophoresis parameter and Hartmann number. The enhancement in Nusselt number and Sherwood number is noticed with the increase in the radiation parameter.

Table 2. Numerical values of $\frac{1}{2}\sqrt{Re_x}$ and $\frac{1}{2}\left(\frac{U_w}{V_w}\right)\sqrt{Re_x, C_{f_y}}$.

S	M	We ₁	We ₂	$\frac{1}{2}\sqrt{Re_x C_{f_x}}$	$\frac{1}{2}\sqrt{Re_x C_{f_y}}$
0.3	0.2	0.3	0.3	1.52872	0.665291
0.4				1.55401	0.678817
0.6				1.60411	0.705454
0.5	0.5			1.54352	0.701708
	1.0			1.82499	0.841934
	1.5			2.16581	1.001912
		0.2		2.18081	1.02175
		0.4		1.50639	1.02206
		0.6		1.53092	1.02391
			0.2	2.23525	1.01810
			0.4	2.23542	1.02798
			0.5	2.23553	1.03688

Table 3. Numerical values of $\frac{N_{u_x}}{\sqrt{Re_x}}$ and $\frac{Sh_x}{\sqrt{Re_x}}$.

Pr	S	Rd	M	Nt	Nb	$\frac{N_{u_x}}{\sqrt{Re_x}}$	$\frac{Sh_x}{\sqrt{Re_x}}$
1.0	0.5	0.4	0.2	0.4	0.6	0.304177	0.041371
0.7						0.677376	0.101602
1.2						0.85375	0.293637
2.0	0.3					0.354678	0.0826865
	0.4					0.387242	0.0606775
	0.6					0.445082	0.0246227
		1.0				0.515614	0.0698414
		1.5				0.591333	0.0828224
		2.0				0.664225	0.091394
			0.5			0.426524	0.0380633
			1.0			0.406532	0.0289907
			1.5			0.397715	0.0192433
				0.2		0.419368	0.0984527
				0.3		0.418316	0.0697986
				0.5		0.41622	0.0131722
					0.7	0.41595	0.0581801
					0.8	0.414637	0.0707656
					0.9	0.41333	0.0805359

7. Concluding Remarks

The optimized model for Carreau nanofluid flow has been predicted by considering the contribution of thermal radiation, external magnetic field, and activation energy. The numerical simulations are performed via shooting technique, and the main findings can be summarized as follows:

- ❖ A reduction in both horizontal and vertical velocity components is noticed when the Weissenberg number and unsteady parameter are increased.

- ❖ With increasing the behavior index and porosity parameter, the flow intensity becomes less important.
- ❖ The temperature profile increases with the Weissenberg number and radiation parameters.
- ❖ Heat transfer is highly affected by the consideration of variable thermal conductivity.
- ❖ Higher concentrations are encountered with an increase in the activation energy and thermophoresis parameters.
- ❖ Entropy generation is more convenient when the Weissenberg number, Brinkman number, and magnetic parameter are increased.
- ❖ The heat and mass transfers are boosted by the increase in the Weissenberg number.

Author Contributions: Conceptualization, S.U.K., I.S., K.G. and L.K.; methodology, S.U.K., I.S. and H.A.; validation, S.U.K., T.L. and I.S.; formal analysis, S.U.K., K.G. and H.A.; investigation, S.U.K., I.S., K.G. and L.K.; writing—original draft preparation, S.U.K., I.S., K.G., H.A., T.L. and L.K.; writing—review and editing S.U.K., I.S., K.G., H.A., T.L. and L.K.; supervision, L.K.; project administration, I.S.; funding acquisition, I.S. All authors have read and agreed to the published version of the manuscript.

Funding: This research project was funded by the Deanship of Scientific Research, Princess Nourah bint Abdulrahman University, through the Program of Research Project Funding After Publication, grant No. (44- PRFA-P-39).

Data Availability Statement: Not applicable.

Conflicts of Interest: The authors declare no conflict of interest.

References

1. Irfan, M.; Rafiq, K.; Khan, M.; Waqas, M.; Anwar, M.S. Theoretical analysis of new mass flux theory and Arrhenius activation energy in Carreau nanofluid with magnetic influence. *Int. Commun. Heat Mass Transf.* **2021**, *120*, 105051. [[CrossRef](#)]
2. Hsiao, K.L. To promote radiation electrical MHD activation energy thermal extrusion manufacturing system efficiency by using Carreau-Nanofluid with parameters control method. *Energy* **2017**, *130*, 486–499. [[CrossRef](#)]
3. Khan, M.I.; Kumar, A.; Hayat, T.; Waqas, M.; Singh, R. Entropy generation in flow of Carreau nanofluid. *J. Mol. Liq.* **2019**, *278*, 677–687. [[CrossRef](#)]
4. Waqas, M.; Khan, M.I.; Hayat, T.; Alsaedi, A. Numerical simulation for magneto Carreau nanofluid model with thermal radiation: A revised model. *Comput. Methods Appl. Mech. Eng.* **2017**, *324*, 640–653. [[CrossRef](#)]
5. Ullah, A.Z.; Guo, X.; Gul, T.; Ali, I.; Saeed, A.; Galal, A.M. Thin film flow of the ternary hybrid nanofluid over a rotating disk under the influence of magnetic field due to nonlinear convection. *J. Magn. Magn. Mater.* **2023**, *573*, 170673. [[CrossRef](#)]
6. Muhammad, K.; Hayat, T.; Alsaedi, A.; Ahmad, B. Melting heat transfer in squeezing flow of base fluid (water), nanofluid (CNTs + water) and hybrid nanofluid (CNTs + CuO + water). *J. Therm. Anal. Calorim.* **2021**, *143*, 1157–1174. [[CrossRef](#)]
7. Rasool, G.; Wakif, A. Numerical spectral examination of EMHD mixed convective flow of second-grade nanofluid towards a vertical Riga plate using an advanced version of the revised Buongiorno's nanofluid model. *J. Therm. Anal. Calorim.* **2021**, *143*, 2379–2393. [[CrossRef](#)]
8. Alqarni, M.S.; Yasmin, S.; Waqas, H.; Khan, S.A. Recent progress in melting heat phenomenon for bioconvection transport of nanofluid through a lubricated surface with swimming microorganisms. *Sci. Rep.* **2022**, *12*, 8447. [[CrossRef](#)]
9. Borbora, M.H.; Vasu, B.; Chamkha, A.J. A Review Study of Numerical Simulation of Lid-Driven Cavity Flow with Nanofluids. *J. Nanofluids* **2023**, *12*, 589–604. [[CrossRef](#)]
10. Acharya, S. Effect of Cavity Undulations and Thermal Boundary Conditions on Natural Convection and Entropy Generation in CuO-Water/Al₂O₃-Water Nanofluid. *J. Nanofluids* **2023**, *12*, 687–698. [[CrossRef](#)]
11. Shamshuddin, M.D.; Salawu, S.O.; Asogwa, K.K.; Rao, P.S. Thermal exploration of convective transportation of ethylene glycol based magnetized nanofluid flow in porous cylindrical annulus utilizing MOS₂ and Fe₃O₄ nanoparticles with inconstant viscosity. *J. Magn. Magn. Mater.* **2023**, *573*, 170663. [[CrossRef](#)]
12. Negi, A.S.; Kumar, A.; Yaseen, M.; Rawat, S.K.; Saini, A. Effects of heat source on the stagnation point flow of a nanofluid over a stretchable sheet with magnetic field and zero mass flux at the surface. *Forces Mech.* **2023**, *11*, 100190. [[CrossRef](#)]
13. Maiti, H.; Mukhopadhyay, S. Existence of MHD boundary layer hybrid nanofluid flow through a divergent channel with mass suction and injection. *Chem. Eng. J. Adv.* **2023**, *14*, 100475. [[CrossRef](#)]
14. Mabood, F.; Khan, S.U.; Tlili, I. Numerical simulations for swimming of gyrotactic microorganisms with Williamson nanofluid featuring Wu's slip, activation energy and variable thermal conductivity. *Appl. Nanosci.* **2020**, *13*, 131–144. [[CrossRef](#)]

15. Makhdom, B.M.; Mahmood, Z.; Fadhl, B.M.; Aldhabani, M.S.; Khan, U.; Eldin, S.M. Significance of entropy generation and nanoparticle aggregation on stagnation point flow of nanofluid over stretching sheet with inclined Lorentz force. *Arab. J. Chem.* **2023**, *16*, 104787. [[CrossRef](#)]
16. Ge-JiLe, H.; Qayyum, S.; Shah, F.; Khan, M.I.; Khan, S.U. Slip flow of Jeffrey nanofluid with activation energy and entropy generation applications. *Adv. Mech. Eng.* **2021**, *13*, 16878140211006578. [[CrossRef](#)]
17. Shah, F.; Khan, S.A.; Al-Khaled, K.; Khan, M.I.; Khan, S.U.; Shah, N.A.; Ali, R. Impact of entropy optimized Darcy-Forchheimer flow in MnZnFe₂O₄ and NiZnFe₂O₄ hybrid nanofluid towards a curved surface. *ZAMM-J. Appl. Math. Mech. Z. Angew. Math. Mech.* **2022**, *102*, e202100194. [[CrossRef](#)]
18. Rajkumar, D.; Reddy, A.S.; Narayana, P.S.; Jagadeshkumar, K.; Chamkha, A.J. Pulsating magnetohydrodynamic flow of Fe₃O₄-blood based micropolar nanofluid between two vertical porous walls with Cattaneo–Christov heat flux and entropy generation. *J. Magn. Magn. Mater.* **2023**, *571*, 170564. [[CrossRef](#)]
19. Derikv, M.; Solari, M.S.; Toghraie, D. Entropy generation and forced convection analysis of ethylene glycol/MWCNTs-Fe₃O₄ non-Newtonian nanofluid in a wavy microchannel with hydrophobic surfaces on. *J. Taiwan Inst. Chem. Eng.* **2023**, *143*, 104707. [[CrossRef](#)]
20. Irfan, M.; Khan, M.; Khan, W.A. Numerical analysis of unsteady 3D flow of Carreau nanofluid with variable thermal conductivity and heat source/sink. *Results Phys.* **2017**, *7*, 3315–3324. [[CrossRef](#)]
21. Hayat, T.; Aziz, A.; Muhammad, T.; Alsaedi, A. Numerical simulation for three-dimensional flow of Carreau nanofluid over a nonlinear stretching surface with convective heat and mass conditions. *J. Braz. Soc. Mech. Sci. Eng.* **2019**, *41*, 55. [[CrossRef](#)]
22. Sharidan, S.; Mahmood, M.; Pop, I. Similarity solutions for the unsteady boundary layer flow and heat transfer due to a stretching sheet. *Appl. Mech. Eng.* **2006**, *11*, 647.
23. Chamkha, A.J.; Aly, A.M.; Mansour, M.A. Similarity solution for unsteady heat and mass transfer from a stretching surface embedded in a porous medium with suction/injection and chemical reaction effects. *Chem. Eng. Commun.* **2010**, *197*, 846–858. [[CrossRef](#)]
24. Shiner, J.S. (Ed.) *Entropy and Entropy Generation: Fundamentals and Applications*; Springer Science & Business Media: Berlin/Heidelberg, Germany, 2001; Volume 18.

Disclaimer/Publisher’s Note: The statements, opinions and data contained in all publications are solely those of the individual author(s) and contributor(s) and not of MDPI and/or the editor(s). MDPI and/or the editor(s) disclaim responsibility for any injury to people or property resulting from any ideas, methods, instructions or products referred to in the content.